Journal Name

ARTICLE

Energy transfer and photoluminescence properties of lanthanide-containing polyoxotitanate cages coordinated by salicylate ligands

Received 00th January 20xx,
Accepted 00th January 20xx

DOI: 10.1039/x0xx00000x

www.rsc.org/

Ning Li,[a,b] Gomathy Sandhya Subramanian,[b] Peter D. Matthews,[a,c] James Xiao,[d] Vijila Chellappan,[b] Timothy E. Rosser,[a] Erwin Reisner,[a] He-Kuan Luo,[b]* and Dominic S. Wright[a]*

Polyoxotitanate (POT) cages have attracted considerable attention recently, much of this from the fact that they can be considered as structural models for the technologically important semiconductor TiO_2. Among the reported POT cages, lanthanide-containing (Ln-POT) cages are of particular interest owing to the fascinating luminescence properties of Ln^{3+} ions and the versatile coordination environments that they can adopt. In the present study, we report the energy transfer mechanism and photoluminescence properties of a series of isostructural Ln-POT cages coordinated by salicylate ligands, of general formula $[LnTi_6O_3(O^iPr)_9(salicylate)_6]$ (**Ln-1**, Ln = La to Er excluding Pm). Both visible (for **Pr-1**, **Sm-1**, **Eu-1**, **Ho-1** and **Er-1**) and near-infrared (for **Nd-1** and **Er-1**) Ln^{3+}-centred photoluminescence can be sensitised in solution, and most importantly, their excitation bands all extend well into the visible region up to 475 nm. With the assistance of steady-state and time-resolved photoluminescence spectroscopy, an energy transfer mechanism involving the salicylate-to-Ti^{4+} charge-transfer state is proposed to account for the largely red-shifted excitation wavelengths of these **Ln-1** cages. The photoluminescence quantum yield of **Nd-1** upon excitation *via* the charge-transfer state reaches 0.30 ± 0.01 % in solution, making it among the highest reported values for Nd^{3+}-complexes in the literature.

Introduction

Inspired by the widespread applications of TiO_2, polyoxotitanate (POT) cages of the type $[Ti_xO_y(OR)_z]$ (OR = alkoxide) have attracted considerable attention in recent years.[1-5] As model compounds, the atomically well-defined POT cages can offer a unique opportunity to bridge the gap between experimental and theoretical studies on the photocatalysis mechanism in titanium oxide systems, as well as to investigate structure-property relations.[6,7] Through heterometallic doping and/or functional ligand modification, we and others have developed a library of POT cages and explored their potential applications.[8-14] In this context, lanthanide-containing polyoxotitanate (Ln-POT) cages possess intriguing structural features and appealing properties,[15-28] due to the diverse coordination environments of the Ln^{3+} ions.[29]

The main reason for general interest in lanthanide complexes is their advantageous luminescence properties, such as long excited state lifetimes, narrow emission bandwidths and excellent resistance to photo-bleaching.[29] Ln^{3+} luminescence mainly originates from the electronic transition within their 4*f* orbitals, but most of these intra-*f* transitions are forbidden according to the Laporte rule. As a result, direct excitation of Ln^{3+} ions is usually inefficient, with extremely low molar extinction coefficients (i.e., 1-10 $M^{-1}cm^{-1}$).[30] This limitation can be overcome with the assistance of highly absorbing '*antenna*' ligands located in close proximity to the Ln^{3+} ions *via* the classic $S_0 \rightarrow S_1 \rightarrow T_1 \rightarrow Ln^{3+}$ energy transfer route.[31] In the literature, the majority of the previous reports on Ln-POT cages, however, have primarily focused on their syntheses and structural characterization,[15-25] leaving the photoluminescence properties less explored. In 2015, Wang *et al* studied the photoluminescence behaviour of anthracenecarboxylate-modified Ln-POT cages (with Ln_2Ti_{10} cores, Ln = Eu and Nd) and investigated the energy transfer process between the ligands and the Ln^{3+} centres.[26] In 2016, Zhang *et al* reported a group of Ln-POT cages (with $LnTi_{11}$ core arrangements, Ln = Sm, Eu and Gd) which could be used as potential molecule-based fluorescent labelling agents.[27] Very recently, Lu *et al* synthesized three Eu^{3+}-containing POT cages (with Eu_2Ti_4, Eu_5Ti_4 and Eu_8Ti_{10} cores) coordinated with 4-*tert*-butylbenzoate, and revealed a size-dependent quantum yield phenomenon in solution.[28] The photophysical interplay between the coordinated ligands, Ln^{3+} centres and Ti^{4+} ions was, unfortunately, not clearly demonstrated in these studies, as the excitation of Ln^{3+} photoluminescence arose either from direct intra-*f* transitions or from the coordinated ligands alone.

[a] Department of Chemistry, University of Cambridge, Lensfield Road, CB2 1EW, UK. *E-mail: dsw1000@cam.ac.uk
[b] Institute of Materials Research and Engineering, Agency for Science, Technology and Research, 2 Fusionopolis Way, 08-03, Innovis, Singapore, 138634. *E-mail: luoh@imre.a-star.edu.sg
[c] School of Chemical and Physical Sciences, Lennard-Jones Building, Keele University, Keele, Staffordshire, ST5 5BG, UK.
[d] Cavendish Laboratory, University of Cambridge, J. J. Thomson Avenue, CB3 0HE, UK.

† Electronic Supplementary Information (ESI) available: UV-Vis absorbance spectra, emission decay profiles, low concentration NMR spectra, proposed energy diagram, etc. See DOI: 10.1039/x0xx00000x

Here we present the energy transfer mechanism and photoluminescence properties of the Ln-POT cages $[LnTi_6O_3(O^iPr)_9(salicylate)_6]$ (**Ln-1**, Ln = La, Ce, Pr, Nd, Sm, Eu, Gd, Tb, Dy, Ho and Er) that we have reported previously.[16] The salicylate-Ti^{4+} moiety is found to be an effective visible light responsive '*antenna*' for Ln^{3+} sensitisation, although salicylate itself is usually considered inefficient in this role.[32-34] Both visible (for **Pr-1**, **Sm-1**, **Eu-1**, **Ho-1** and **Er-1**) and NIR (for **Nd-1** and **Er-1**) photoluminescence can be sensitised by visible light excitation up to 475 nm, representing a special example in which one visible-responsive ligand system is suitable for Ln^{3+} ion sensitisation across the visible-NIR spectrum.[35-39] The charge-transfer process from salicylate HOMO to Ti^{4+} *d* orbitals is proposed to account for the largely red-shifted excitation wavelengths, supported by both steady-state and time-resolved photoluminescence spectral data.

Results and Discussion

The common molecular structure of **Ln-1** possesses a C_3-symmetric $LnTi_6O_3$ core with six tridentate salicylate ligands at the periphery (Fig. 1a and 1b).[16] The six-coordinate Ti^{4+} ions form a shell encapsulating the nine-coordinate Ln^{3+} centre, in which TiO_6 octahedra and LnO_9 distorted tricapped trigonal prism assemble into an edge-sharing polyhedral arrangement (Fig. 1c). The topology of **Ln-1** has several advantages over other lanthanide complexes in which direct coordination of aromatic ligands to the Ln^{3+} ion occurs: (*i*) the encapsulation of Ln^{3+} by diamagnetic Ti^{4+} ions significantly enlarges the distance between the Ln^{3+} ions and the X-H (X = C or O) oscillators located on solvent molecules or peripheral ligands, thus giving high intrinsic quantum yields;[38] (*ii*) the firm embedding of the Ln^{3+} ions within **Ln-1** is also potentially beneficial for *in vivo* biological applications where the cytotoxicity of heavy metal ions is usually critical;[40,41] (*iii*) the isopropoxide ligands can be easily replaced by other ligands, which could promote more versatile functionalities.[1]

The phase purity of these **Ln-1** cages was initially confirmed by the satisfactory agreement between their experimental and simulated powder XRD patterns (Fig. 2a and 2b). All these **Ln-1** cages demonstrate similar absorbance spectra (Fig. S1, ESI). As shown in Figure 2c, **Gd-1**, being a representative of the **Ln-1** family, exhibits intense absorption in a wavelength range up to 475 nm, within which an absorption edge at 250 - 300 nm and a broad band centred at *ca.* 350 nm are observed. The 350 nm absorption band is due to the charge-transfer process from the salicylate HOMO level to Ti^{4+} *d* orbitals. This was confirmed by a control experiment in which a shoulder at similar wavelengths emerges upon mixing salicylic acid with $Ti(O^iPr)_4$ in *n*-pentane (Fig. 2c, blue trace), and is further supported by the similar charge-transfer behaviour observed for a number of other ligand-modified POT cages and TiO_2 nanoparticles.[12,42] The absorption edge at 250 - 300 nm can be attributed to the $O^{2-} \rightarrow Ti^{4+}$ transition in the Ti_xO_y core, which is also a commonly observed feature for many POT cages.[12] Salicylic acid alone has an absorption band centred at *ca.* 310 nm arising from its transition from ground to singlet excited state ($S_0 \rightarrow S_1$). Upon excitation at 300 nm in solution, salicylic acid exhibits a broad emission band located at *ca.* 440 nm (Fig. 2d), which can be assigned to the fluorescence from the S_1 state.

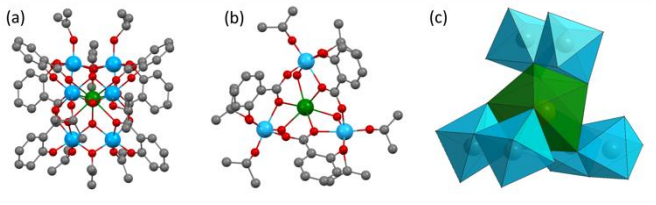

Fig. 1. Ball and stick representation of the molecular structure of $[LnTi_6O_3(O^iPr)_9(salicylate)_6]$ (a) perpendicular to and (b) along the C_3 symmetry axis; (c) the polyhedral representation of the cage core containing six Ti-octahedra and one Ln-tricapped trigonal prism polyhedron. Colour code for atoms: Ti = cyan, Ln = green, O = red, C = grey. Hydrogen atoms are omitted for clarity.

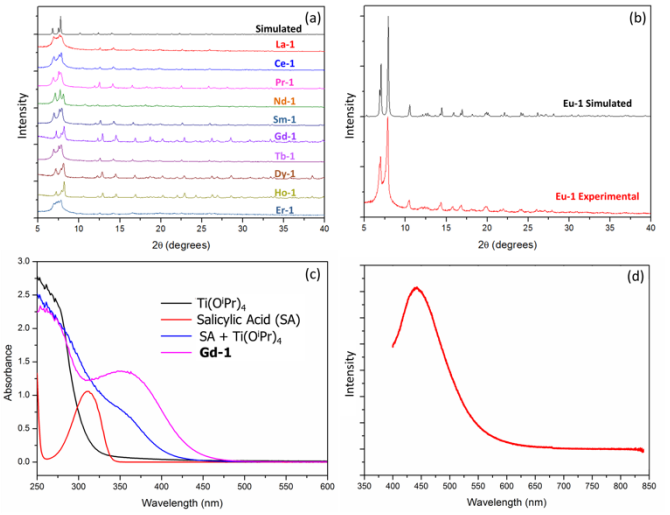

Fig. 2. (a) Comparison of simulated and experimental pXRD patterns of **Ln-1** cages except for **Eu-1**; simulated spectrum is from the single-crystal diffraction data of **La-1**, but that of other **Ln-1** cages are all similar since they are isostructural. (b) Comparison of the simulated and experimental pXRD patterns of **Eu-1**. (c) The absorbance spectra of $Ti(O^iPr)_4$ (black), salicylic acid (red), mixture of salicylic acid and $Ti(O^iPr)_4$ (blue), and **Gd-1** (*ca.* 40 μM, pink) in anhydrous *n*-pentane. (d) The steady-state photoluminescence spectrum of salicylic acid in anhydrous *n*-pentane with 300 nm excitation. All measurements were performed at room temperature

Among the eleven **Ln-1** cages in this study, only six (**Pr-1**, **Nd-1**, **Sm-1**, **Eu-1**, **Ho-1** and **Er-1**) show detectable Ln^{3+}-centred intra-*f* transition photoluminescence peaks in the visible-NIR range (Fig. 3a). Upon monitoring the most intense Ln^{3+}-centred emission signals, similar excitation spectra were recorded for all these **Ln-1** cages, consisting of a minor band centred at *ca.* 300 nm and a major one at *ca.* 400 nm, as well as some intra-*f* transition peaks (Fig. 3a). The relatively lower intensity of the intra-*f* peaks suggests more efficient sensitisation *via* the '*antenna*' ligands, compared to direct intra-*f* transitions. Upon excitation at 405 nm, bright red/pink coloured luminescence can be clearly seen from **Pr-1**, **Sm-1** and **Eu-1** solutions by the naked eye (Fig. S2, ESI).

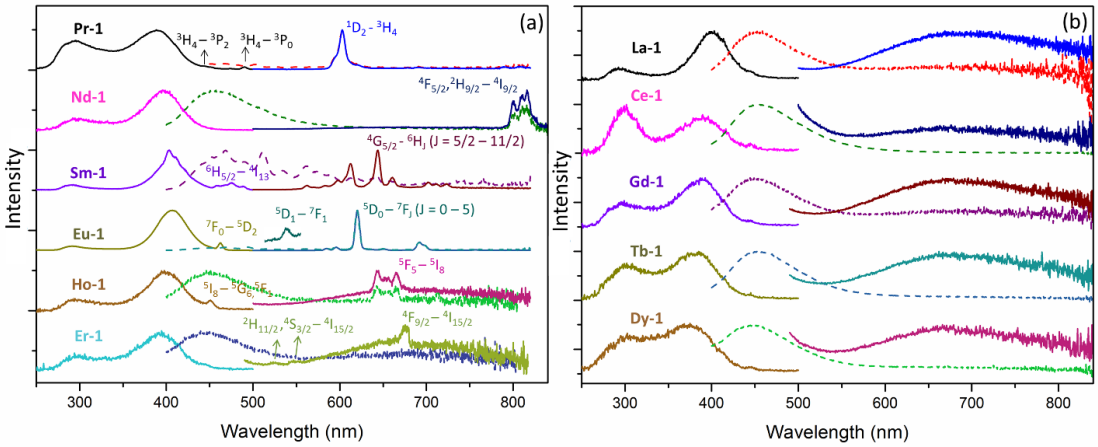

Fig. 3. Normalized excitation and steady-state emission spectra of **Ln-1** compounds: (a) those showing Ln^{3+}-centred signals (i.e., **Pr-1**, **Nd-1**, **Sm-1**, **Eu-1**, **Ho-1** and **Er-1**), and (b) those only showing ligand-centred signals (i.e., **La-1**, **Ce-1**, **Gd-1**, **Tb-1** and **Dy-1**). Excitation spectra were recorded by monitoring the most intense Ln^{3+}-centred emission peaks [for (a)] or emission at 650 nm [for (b)]. Two emission spectra are shown for each compound, which were excited at the *ca.* 300 nm (dashed line) and *ca.* 400 nm excitation band (solid line), respectively. The Ln^{3+} intra-*f* transitions peaks are also indicated. Of note, the peaks in the 450 - 500 nm range in the emission spectrum of **Sm-1** in (a) are residual signals from the Xenon light source, which is also present in the emission spectra of **Pr-1** and **Eu-1** at similar wavelengths (only visible upon zooming in), but obscured by the broad ligand-centred emission band at *ca.* 450 nm for other **Ln-1** members.

The minor excitation band centred at *ca.* 300 nm matches the absorbance spectrum of deprotonated salicylic acid, which is slightly blue-shifted compared with the protonated molecule.[43] Therefore, this band can be attributed to the excitation of the salicylate ligand, undergoing a $S_0 \rightarrow S_1$ transition at this excitation wavelength.[32-34] Apart from the Ln^{3+}-centred emission, excitation at 300 nm also leads to a broad emission band at *ca.* 450 nm for **Nd-1**, **Sm-1**, **Ho-1** and **Er-1**, corresponding to the fluorescence of salicylate S_1 state.[44] This result suggests incomplete energy transfer from salicylate to Ln^{3+} emissive states. In addition, it is worth mentioning that the $O^{2-} \rightarrow Ti^{4+}$ transition might also play a role in the minor excitation band at *ca.* 300 nm, since a similar excitation mechanism has been revealed in solid-state Ln-doped TiO_2 materials.[45]

What makes these **Ln-1** compounds unique is the presence of the major excitation band in the region of 350 - 475 nm with the peak position at around 400 nm (Fig. 3a). In general, UV excitation to visible/NIR emission or visible excitation to NIR emission are common for Ln^{3+}-containing complexes, but the visible excitation to visible emission process observed here is relatively rare and usually needs sophisticated ligands design.[46] Moreover, the salicylate ligand itself is usually considered inefficient for the sensitisation of Ln^{3+} ions, because the energy levels of its excited states are too high and the excitation window is limited only to the UV range. In this case, by coordinating with Ti^{4+} ions we have turned salicylate into an effective and visible light responsive ligand for Ln^{3+} photoluminescence sensitisation.

The remaining five cages (**La-1**, **Ce-1**, **Gd-1**, **Tb-1** and **Dy-1**) only show ligand-centred emission bands at *ca.* 450 nm with 300 nm excitation, as well as an extremely broad feature in the 550 - 800 nm region with either 300 or 400 nm excitation (Fig. 3b). Solely ligand-centred emission is expected for **La-1**, **Ce-1** and **Gd-1** because they do not have any intra-*f* transitions within the visible-NIR range. However, it is surprising that neither Tb^{3+} nor Dy^{3+} photoluminescence signals were detected, despite the fact that they are very well-known green and yellow light emitters.[47] The excitation spectra of these five cages were recorded at different emission wavelengths from 700 nm to 550 nm (in 50 nm steps) (Fig. S3 and S4, ESI). The intensity of the major excitation band (*ca.* 400 nm) decreases, with the emission wavelength shifting towards the blue direction for each of the compounds, clearly suggesting that the broad feature in the 550 - 800 nm range corresponds to the excitation band at *ca.* 400 nm.

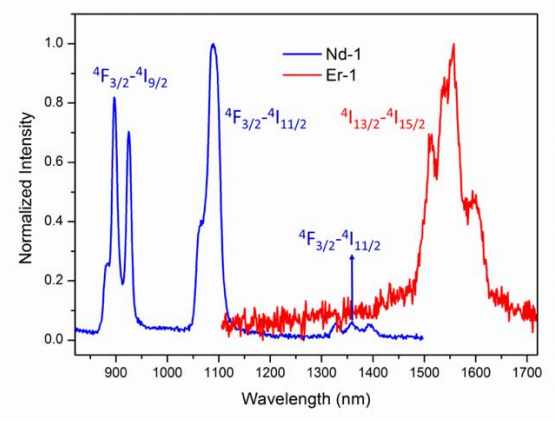

Fig. 4. Normalized steady-state NIR emission spectra of **Nd-1** and **Er-1** in anhydrous *n*-pentane upon 405 nm laser excitation. Intra-*f* transition peaks are indicated.

The steady-state NIR (1000 - 1800 nm) emission spectra of **Ln-1** were also recorded, with only **Nd-1** and **Er-1** showing detectable Ln^{3+}-centred emission peaks upon 405 nm laser excitation (Fig. 4). Because neither Nd^{3+} nor Er^{3+} have intra-*f* transitions with energy gaps corresponding to the 405 nm wavelength, the excitation must be *via* the '*antenna*' ligands.[48] The photoluminescence quantum yields for **Ln-1** in *n*-pentane

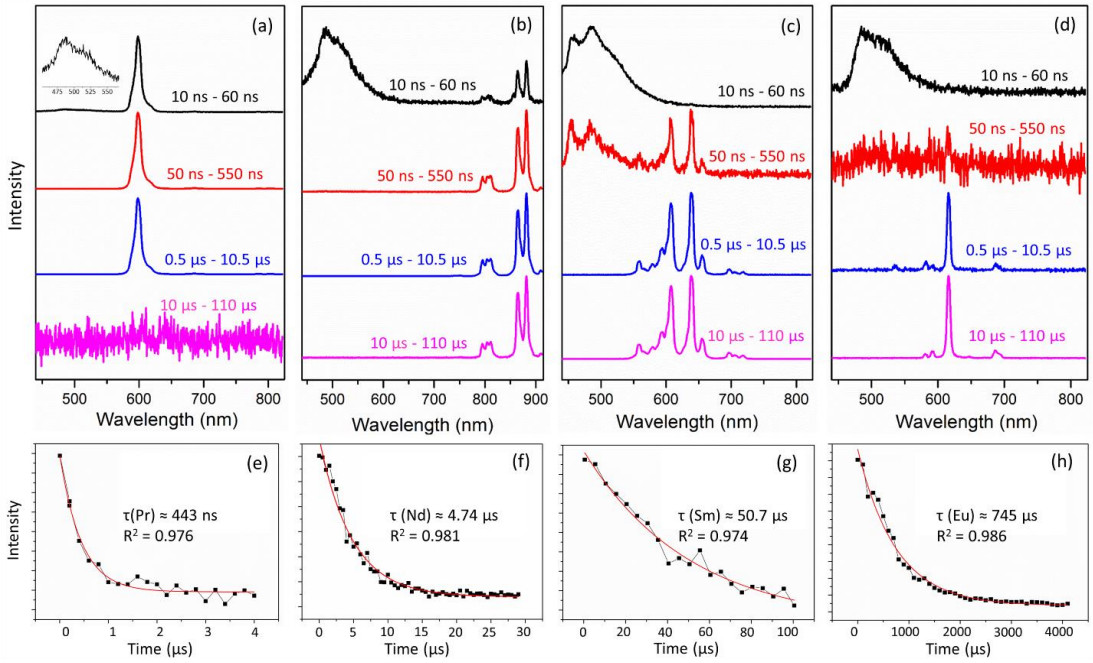

Fig. 5. The time-resolved emission spectra of (a) **Pr-1**, (b) **Nd-1**, (c) **Sm-1** and (d) **Eu-1** at different intervals after laser pulse excitation at 430 nm: 10 ns - 60 ns (black), 50 ns - 550 ns (red), 0.5 µs - 10.5 µs (blue) and 10 µs - 110 µs (pink). The Ln^{3+}-centred emission decay profile of (e) **Pr-1**, (f) **Nd-1**, (g) **Sm-1** and (h) **Eu-1**. The estimated lifetimes are also shown

solution were measured using the integration sphere method,[49] giving 0.037 ± 0.003 % for **Eu-1** (using 405 nm excitation and $^5D_0 \rightarrow {}^7F_2$ emission) and 0.30 ± 0.01 % for **Nd-1** (using 405 nm excitation, $^4F_{3/2} \rightarrow {}^4I_{9/2}$ and $^4F_{3/2} \rightarrow {}^4I_{11/2}$ emissions); the values for other **Ln-1** members are all below the sensitivity of the equipment employed. It is worth noting that the quantum yield of **Nd-1** (0.30 ± 0.01 %) represents one of the highest values for Nd^{3+}-complexes reported in the literature,[50] suggesting an efficient energy transfer process.

To establish the energy transfer mechanism within these species, time-resolved emission spectra of **Pr-1**, **Nd-1**, **Sm-1** and **Eu-1** were recorded at different time intervals (i.e., 10 ns - 60 ns, 50 ns - 550 ns, 0.5 µs -10.5 µs and 10 µs -110 µs) after the excitation laser pulse at 430 nm. In addition to the different rising/decaying kinetics of the Ln^{3+} emission signals, perhaps the most striking feature is the appearance of a new broad band at *ca.* 500 nm observed for **Pr-1**, **Nd-1**, **Sm-1** and **Eu-1** in the interval of 10 ns - 60 ns (Fig. 5). Similar emission band is also present for the other seven **Ln-1** members in the same time interval after the laser pulse (Fig. 6), suggesting its origin is the salicylate-Ti^{4+} moieties in the **Ln-1** structure. To prevent potential interference from the residual light source, a long-pass optical filter with 515 nm cut-off was placed between the sample and the CCD detector, and the red edge of the emission band can still be observed, confirming the close correlation between the *ca.* 400 nm excitation and the *ca.* 500 nm emission bands. Lifetimes of the emission at 525 nm were measured with the optical filter in place. The obtained lifetimes might not be accurate, because they are all close to the response time of the equipment employed (Fig. S5, ESI).

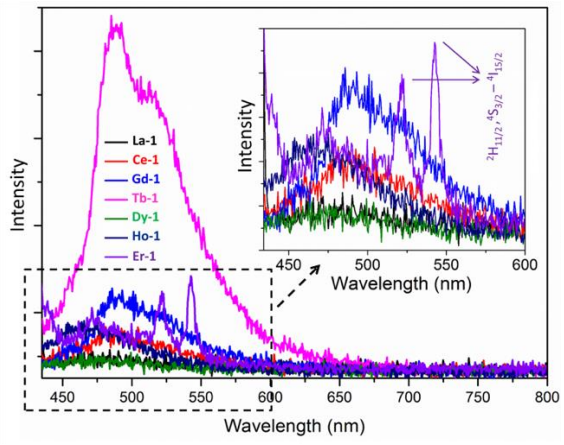

Fig. 6. Emission spectra of **Ln-1** in the 10 ns - 60 ns time interval after the 430 nm laser excitation pulse. Inset is the magnification of the low intensity area. Intra-*f* transition peaks are observed for **Er-1** and indicated in the figure inset

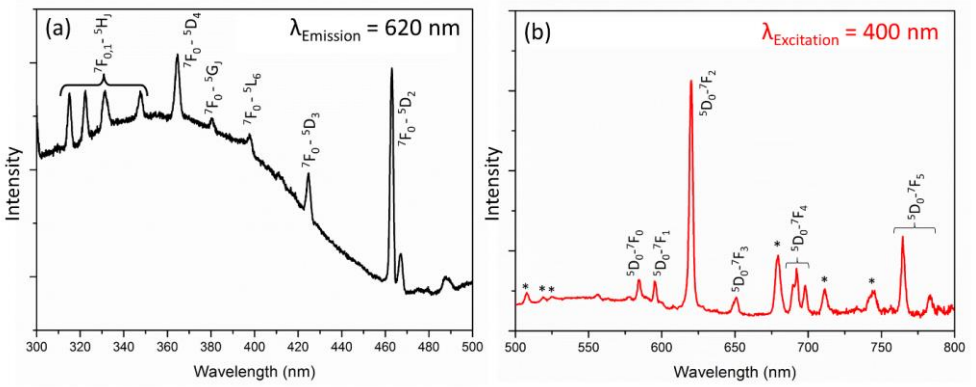

Fig. 7. Photoluminescence excitation (a) and emission (b) spectra of **Eu-1** in the solid-state. The intra-*f* transitions corresponding to Eu^{3+} ions are indicated. The peaks marked with '*' are possibly from the scattering of the light source, as their positions change with the excitation wavelengths (see Figure S7 in the ESI).

As a comparison, the photoluminescence excitation and emission spectra of solid-state **Eu-1** crystals were also recorded (Fig. 7). Upon excitation at 400 nm, signature emission signals of Eu^{3+} ion can be clearly observed and unambiguously assigned to the $^5D_0 \rightarrow {}^7F_J$ (J = 0 - 5) transitions. Because the intensity of the Eu^{3+} $^5D_0 \rightarrow {}^7F_2$ emission (electrical dipole transition) varies strongly with the local symmetry, while that of the $^5D_0 \rightarrow {}^7F_1$ emission (magnetic dipole transition) is independent on the local environment, the intensity ratio of these two signals can be employed to probe the local coordination environment of Eu^{3+}.[28] In this case, the ratio for **Eu-1** solid-state sample was determined to be around 14.8, satisfactorily matching with that from solution (i.e., *ca.* 14.9). This result supports the hypothesis that there is no change of local symmetry around Eu^{3+}. Furthermore, the NMR spectra of diamagnetic **La-1** compound (as an example of the **Ln-1** family) at low concentration was also recorded, which shows similar peak positions and splitting patterns to the high concentration sample (Fig. S6, ESI). These results indicate the cage structure of **Ln-1** remains *intact* in dilute solutions, and the red-shifted excitation wavelengths, therefore, originate from the unique molecular structure of the cages.

The excitation spectrum of solid-state **Eu-1** upon monitoring the $^5D_0 \rightarrow {}^7F_2$ emission at 620 nm exhibits a number of intra-*f* transition peaks and a broad band centred at *ca.* 350 nm. This 350 nm excitation band differs from that of the **Eu-1** solution sample (i.e., major excitation band at *ca.* 400 nm and minor band at *ca.* 300 nm, Fig. 3a), but it is in line with the intense absorption at similar wavelengths, corresponding to the salicylate HOMO level-to-Ti^{4+} charge-transfer state (Fig. 2c and S1).

In view of all this experimental evidence, we propose that the largely red-shifted excitation is a result of the salicylate to Ti^{4+} charge-transfer (i.e., ligand-to-metal charge-transfer, LMCT) process, which dramatically lowers the energy required for Ln^{3+} photoluminescence sensitisation. As shown in Fig. 8 left panel, upon coordination of salicylate ligand with the Ti^{4+} ion, electrons can be transferred through either the salicylate HOMO → LUMO → Ti^{4+} route or directly from salicylate HOMO to Ti^{4+} *d* orbitals. The latter requires a much lower energy to trigger the charge-transfer process. This is also the reason why the **Ln-1** compounds are all bright yellow in colour, although both Ti^{4+} and salicylic acid are colourless. Despite the fact that a similar charge-transfer process has been widely observed in many other ligand-modified POT cages and TiO_2 nanoparticles,[12,42] its use to sensitise Ln^{3+} photoluminescence in Ln-POT cages has not been revealed before.

The reasons behind the mismatch between the excitation spectra in solution (two bands at *ca.* 300 nm and 400 nm) and in the solid-state (single band at *ca.* 350 nm) samples are unknown yet. One possibility is that the LMCT possesses multiple excited states S_n (n ≥ 1), similar to other organic ligands. In the absorption spectrum of the cages in solution, all these excited states overlap into the broad band centred at *ca.* 350 nm. However, only the lowest excited state S_1, corresponding to the excitation band at *ca.* 400 nm, contributes to the Ln^{3+} luminescence sensitisation, and others (S_n, n ≥ 2) are dissipated to the surrounding environment *via* molecular motion and vibration. In the solid-state sample, the cage molecules are densely packed and their molecular motion/vibration is much restricted so that all of the excited states can now be used to sensitise Ln^{3+} luminescence.

Since the emission band at *ca.* 500 nm and the broad feature at 550 - 800 nm are both associated with the LMCT excitation band at *ca.* 400 nm, we believe they are from the singlet and triplet excited levels of the proposed charge-transfer state, denoted as S_{1ST} and T_{1ST}, respectively. In other words, both fluorescence and phosphorescence can be simultaneously observed at room temperature in the **Ln-1** solution, which is expected for coordination compounds containing heavy atoms (i.e., lanthanides in the present case) because of the strong metal-induced spin-orbit coupling.[51,52] The assignment of the broad feature to phosphorescence is further supported by its higher intensity for **Gd-1** and **La-1** than the other **Ln-1** cages (Fig. S8, ESI). Since Gd^{3+} possesses an extremely high acceptor energy level at *ca.* 32000 cm^{-1} and La^{3+} does not have any *f* electrons ($^4f_0$), energy transfer from ligand to Gd^{3+} or La^{3+} ion is impossible, leaving a high likelihood that the excited energy is relaxed *via* the triplet phosphorescence process. Moreover, the relatively higher

phosphorescence intensity for **Gd-1** over **La-1** can be explained by the fact that the degree of mixing of the singlet and triplet states in **Gd-1** is greater than that in **La-1**. This is due to the higher paramagnetism of Gd^{3+}, as Gd^{3+} has seven uncoupled electrons in the 4*f* sub-shell whereas La^{3+} has none (thus diamagnetic). Unfortunately, the broad feature at 550 - 800 nm could only be seen in the steady-state measurements but not in the time-resolved system. This could be due to the fact that in steady-state measurements there is continuous population of the excited states with a xenon lamp source and yet the emission intensity is still low; whereas in the time-resolved system, only a ns-pulsed laser with a frequency of 1 Hz was used, which should lead to an even lower population of the excited states.

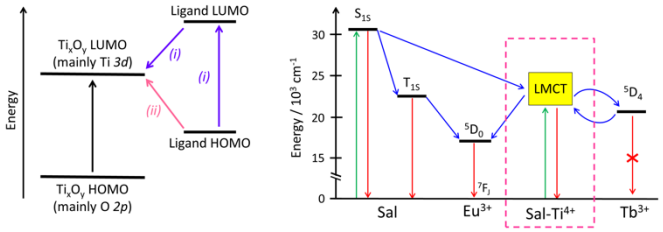

Fig. 8. Left panel: charge-transfer pathways in ligand modified POT cages; *(i)* ligand HOMO→ LUMO→ Ti^{4+} *d* orbital and *(ii)* ligand HOMO→ Ti^{4+} *d* orbital. Right panel: proposed energy transfer mechanism for **Ln-1** cages. **Eu-1** and **Tb-1** are shown as representatives. Green, red and blue arrows indicate excitation, emission and non-radiative energy transfer processes, respectively. The LMCT state and its related energy transfer routes are highlighted by a pink dash-line box.

The proposed energy transfer mechanism involving the LMCT state in the **Ln-1** cages is shown in the right panel of Fig. 8, using **Eu-1** as an example in which sensitised Ln^{3+}-centred luminescence occurs (also for **Pr-1**, **Nd-1**, **Sm-1**, **Ho-1** and **Er-1**) and **Tb-1** as an example where this is not observed (for **Dy-1** as well; a detailed energy level diagram containing the proposed LMCT and emissive states of respective Ln^{3+} ions can be found in Fig. S9, ESI). The energy level of the LMCT state relative to the ground can be estimated to be 21050 cm^{-1} using the red edge of the absorption band (i.e., 475 nm).[39] Upon excitation into the major excitation band at *ca.* 400 nm, the system is firstly excited to the proposed LMCT state before subsequent energy migration to the Eu^{3+} emissive state (i.e., $^5D_0$ at *ca.* 17500 cm^{-1}). However, the LMCT state is too low to facilitate energy transfer to the Tb^{3+} $^5D_4$ emissive state (i.e., *ca.* 20500 cm^{-1}), resulting in the absence of Tb^{3+}-centred emission signals.

Conclusions

In conclusion, we have systematically investigated the energy transfer mechanism and photoluminescence properties of a series of lanthanide-containing polyoxotitanate cages coordinated by salicylate ligands, $[LnTi_6O_3(O^iPr)_9(salicylate)_6]$ (**Ln-1**, Ln = La, Ce, Pr, Nd, Sm, Eu, Gd, Tb, Dy, Ho and Er). Both visible (from **Pr-1**, **Sm-1**, **Eu-1**, **Ho-1** and **Er-1**) and near infrared (from **Nd-1** and **Er-1**) photoluminescence can be sensitised *via* an excitation band in the visible range up to 475 nm. With the assistance of steady-state and time-resolved photoluminescence spectroscopy, an energy transfer mechanism involving salicylate HOMO to Ti^{4+} *d* orbital charge-transfer state is proposed to account for the red-shifted excitation wavelengths of Ln-POT cages. Through the proposed excitation channel, the photoluminescence quantum yield of Nd^{3+} reaches 0.30 ± 0.01 % for **Nd-1** in solution, representing one of the highest reported values in the literature for a Nd^{3+}-complex. This study, we believe, is a significant step forward for understanding the photophysics of lanthanide-containing polyoxotitanate cages coordinated with organic ligands, and should stimulate further interest in related research fields.

Experimental Section

Syntheses

The **Ln-1** cages were synthesized by a solvent-free method described elsewhere.[16] In brief, $Ti(O^iPr)_4$ (5.0 mL, 16.8 mmol), $LnCl_3$ or $LnCl_3{\cdot}xH_2O$ (0.5 mmol) and salicylic acid (345 mg, 2.5 mmol) were mixed in a Teflon-lined autoclave under N_2 environment and heated at 150 °C for three days. Gradually cooling to 40 °C, retaining this temperature for another two days before further cooling to room temperature produced crystalline blocks of **Ln-1** directly from the reaction mixtures (except for **Er-1**). **Er-1** single crystals were grown by adding 3.0 mL of anhydrous THF to the obtained reaction mixture and storing at -30 °C for a week. The crystals were filtered off at room temperature, washed with anhydrous isopropanol, dried *in vacuo* and stored in a N_2-filled glovebox prior to further characterizations. All the utilized chemicals and reagents were obtained from commercial sources and used as received unless otherwise stated.

Sample Preparation

Samples for UV-Vis absorbance measurements were prepared by dissolving the desired amount of high-purity crystalline blocks of **Ln-1** in anhydrous chloroform (Figure S1), whereas the samples for photoluminescence studies were prepared in anhydrous *n*-pentane, since *n*-pentane was found to give the best excitation spectra and it is a non-coordinating solvent. The solubility of **Ln-1** in anhydrous *n*-pentane is poor and also dependent on the choice of Ln^{3+} ion, making it difficult to precisely control the concentration. Therefore, the solution samples for photoluminescence studies were prepared by adding a few high-purity **Ln-1** crystalline blocks (*ca.* 5 mg) into 3.0 mL anhydrous *n*-pentane and incubating for three minutes at room temperature before decanting the clear solutions from the remaining undissolved solid (more than half of the original amount) to a quartz cuvette with a 10 mm path-length. We estimate that the solution concentration for photoluminescence measurements is approximately in the range of 50 - 400 μM, depending on the Ln^{3+} ions. We further found that the excitation and emission spectra are not sensitive to the amount of **Ln-1** used (within the range of a few

milligrams) and the incubation time (within the range of a few minutes). All the manipulations were carried out in a N_2-filled glovebox in order to ensure that there was no possibility of aerial hydrolysis of **Ln-1**, which would give aggregated clusters in solution and/or lanthanide-doped bulk titanium oxide.

Sample Characterization

The UV-Vis absorbance spectra were obtained using a VARIAN Cary 50 Bio UV-Visible Spectrophotometer. The steady-state photoluminescence data in the visible range was obtained using an Edinburgh Instruments FS5 spectrofluorometer with a monochromated xenon lamp as the light source. All the excitation spectra were corrected for the varied xenon lamp intensity. The steady-state photoluminescence measurements in the NIR region were performed using a Coherent OBIS 405 nm laser for excitation. The luminescence emission was focused into an Andor SOLIS spectrometer, using an InGaAs CCD detector. The photoluminescence quantum yields were measured using the integrating sphere method. Time-resolved photoluminescence studies were carried out using an Edinburgh Instrument flash-photolysis spectrometer LP920 equipped with an Edinburgh Instrument LP920-K PMT detector and a time-gated Andor DH720 CCD camera. All the measurements were conducted at room temperature under N_2 atmospheric condition unless otherwise stated.

Conflicts of interest

There are no conflicts to declare.

Acknowledgements

We thank the A*STAR Graduate Scholarship (Overseas) (N. L.), ESPRC (Doctoral Prize for P. D. M. and DTA studentship for T. E. R.), NanoDTC Cambridge EP/L105978/1 (J. X.), the Christian Doppler Research Association and OMV Group (T. E. R. and E. R.) for financial support.

Notes and references

1. L. Rozes, C. Sanchez, *Chem. Soc. Rev.*, 2011, **40**, 1006.
2. P. Coppens, Y. Chen, E. Trzop, *Chem. Rev.,* 2014, **114**, 9645.
3. W.-H. Fang, L. Zhang, J. Zhang, *Chem. Soc. Rev.,* 2018, **47**, 404.
4. M.-Y. Gao, F. Wang, Z.-G. Gu, D.-X. Zhang, L. Zhang, J. Zhang, *J. Am. Chem. Soc.,* 2016, **138**, 2556.
5. W.-H. Fang, L. Zhang, J. Zhang, *J. Am. Chem. Soc.,* 2016, **138**, 7480.
6. J. B. Benedict, P. Coppens, *J. Am. Chem. Soc.,* 2010, **132**, 2938.
7. R. C. Snoeberger III, K. J. Young, J. Tang, L. J. Allen, R. H. Crabtree, G. W. Brudvig, P. Coppens, V. S. Batista, J. B. Benedict, *J. Am. Chem. Soc.,* 2012, **134**, 8911.
8. Y. Lv, J. Cheng, A. Steiner, L. Gan, D. *S. Wright, Angew. Chem. Int. Ed.,* 2014, **53**, 1934.
9. J.-X. Liu, M.-Y. Gao, W.-H. Fang, L. Zhang, J. Zhang, *Angew. Chem. Int. Ed.,* 2016, **55**, 5160.
10. N. Li, P. D. Matthews, J. J. Leung, T. C. King, P. T. Wood, H.-K. Luo, D. S. Wright, *Dalton Trans.,* 2015, **44**, 19090.
11. P. D. Matthews, T. C. King, D. S. Wright, *Chem. Commun.,* 2014, **50**, 12815.
12. N. Li, P. D. Matthews, H.-K. Luo, D. S. Wright, *Chem. Commun.,* 2016, **52**, 11180.
13. S. Hanf, P. D. Matthews, N. Li, H.-K. Luo, D. S. Wright, *Dalton Trans.,* 2017, **46**, 578.
14. Y. Lv, J. Willkomm, A. Steiner, L. Gan, E. Reisner, D. S. Wright, *Chem. Sci.,* 2012, **3**, 2470.
15. M. Moustiakimov, M. Kritikos, G. Westin, *Acta Cryst.,* 1998, **C54**, 29.
16. N. Li, R. García-Rodríguez, P. D. Matthews, H.-K. Luo, D. S. Wright, *Dalton Trans.,* 2017, **46**, 4287.
17. G. Westin, R. Norrestam, M. Nygren, M. Wijk, *J. Solid State Chem.,* 1998, **135**, 149.
18. L. G. Hubert-Pfalzgraf, V. Abada, J. Vaissermann, *Polyhedron,* 1999, **18**, 3497.
19. E. Berger, G. Westin, *J. Sol-Gel Sci.Technol.,* 2010, **53**, 681.
20. C. Artner, S. Kronister, M. Czakler, U. Schubert, *Eur. J. Inorg. Chem.,* 2014, 5596.
21. D.-F. Lu, X.-J. Kong, T.-B. Lu, L.-S. Long, L.-S. Zheng, *Inorg. Chem.,* 2017, **56**, 1057.
22. Y. Lv, Z. Cai, D. Yan, C. Su, W. Li, W. Chen, Z. Ren, Y. Wei, O. Mi, C. Zhang, D. S. Wright, *RSC Adv.,* 2016, **6**, 57.
23. Y. Lv, M. Yao, J. P. Holgado, T. Roth, A. Steiner, L. Gan, R. M. Lambert, D. S. Wright, *RSC Adv.,* 2013, **3**, 13659.
24. Y. Lv, W. Du, Y. Ren, Z. Cai, K. Yu, C. Zhang, Z. Chen, D. S. Wright, *Inorg. Chem. Front.,* 2016, **3**, 1119.
25. Y. Lv, J. Willkomm, M. Leskes, A. Steiner, T. C. King, L. Gan, E. Reisner, P. T. Wood, D. S. Wright, *Chem. Eur. J.,* 2012, **18**, 11867.
26. S. Wang, H.-C. Su, L. Yu, X.-W. Zhao, L.-W. Qian, Q.-Y. Zhu, J. Dai, *Dalton Trans.,* 2015, **44**, 1882.
27. G.-L. Zhang, S. Wang, J.-L. Hou, C.-J. Mo, C.-J. Que, Q.-Y. Zhu, J. Dai, *Dalton Trans.,* 2016, **45**, 17681.
28. D.-F. Lu, Z.-F. Hong, J. Xie, X.-J. Kong, L.-S. Long, L.-S. Zheng, *Inorg. Chem.,* 2017, **56**, 12186.
29. J. C. G. Bünzli, C. Piguet, *Chem. Soc. Rev.,* 2005, **34**, 1048.
30. S. I. Klink, H. Keizer, F. C. J. M. van Veggel, *Angew. Chem. Int. Ed.,* 2000, **39**, 4319.
31. R. D. Archer, H. Chen, *Inorg. Chem.,* 1998, **37**, 2089.
32. M.-C. Yin, L.-J. Yuan, C.-C. Ai, C.-W. Wang, E.-T. Yuan, J.-T. Sun, *Polyhedron,* 2004, **23**, 529.
33. G. Sharma, A. K. Narula, *J. Fluoresc.,* 2015, **25**, 355.
34. G. Kaur, S. B. Rai, *J. Phys. D: Appl. Phys.,* 2011, **44**, 425306.
35. S. Biju, Y. K. Eom, J.-C. G. Bünzli, H. K. Kim, *J. Mater. Chem. C,* 2013, **1**, 3454.
36. G.-L. Law, T. A. Pham, J. Xu, K. N. Raymond, *Angew. Chem. Int. Ed.,* 2012, **51**, 2371.
37. N. Wartenberg, O. Raccurt, E. Bourgeat-Lami, D. Imbert, M. Mazzanti, *Chem. Eur. J.,* 2013, **19**, 3477.
38. S. Quici, M. Cavazzini, G. Marzanni, G. Accorsi, N. Armaroli, B. Ventura, F. Barigelletti, *Inorg. Chem.,* 2005, **44**, 529.
39. C. Y. Chow, S. V. Eliseeva, E. R. Trivedi, T. N. Nguyen, J. W. Kampf, S. Petoud, V. L. Pecoraro, *J. Am. Chem. Soc.,* 2016, **138**, 5100.
40. K. T. Rim, K. H. Koo, J. S. Park, *Health Work,* 2013, **4**, 12.
41. S. Hirano, K. T. Suzuki, *Environmental Health Perspectives,* 1996, **104**, 85.
42. P.-J. Tseng, C.-Y. Wang, T.-Y. Huang, Y.-Y. Chuang, S.-F. Fu, Y.-W. Lin, *Anal. Methods,* 2014, **6**, 1759.
43. H.-B. Guo, F. He, B. Gu, L. Liang, J. C. Smith, *J. Phys. Chem. A,* 2012, **116,** 11870.
44. P. B. Bisht, H. B. Tripathi, D. D. Pant, *J. Photochem. Photobiol. A: Chem.,* 1995, **90**, 103.
45. Ž. Antić, R. M. Krsmanović, M. G. Nikolić, M. Marinović-Cincović, M. Mitrić, S. Polizzi, M. D. Dramićanin, *Materials Chemistry and Physics*, 2012, **135**, 1064.

46. F. J. Steemers, W. Verboom, D. N. Reinhoudt, E. B. van der Tol, J. W. Verhoeven, *J. Am. Chem. Soc.,* 1995, **117**, 9408.
47. K. Binnemans, *Chem. Rev.,* 2009, **109**, 4283.
48. W. Luo, J. Liao, R. Li, X. Chen, *Phys. Chem. Chem. Phys.,* 2010, **12**, 3276.
49. J. C. de Mello, H. F. Wittmann, R. H. Friend, *Adv. Mater.,* 1997, **9**, 230.
50. E. R. Trivedi, S. V. Eliseeva, J. Jankolovits, M. M. Olmstead, S. Petoud, V. L. Pecoraro, *J. Am. Chem. Soc.,* 2014, **136**, 1526.
51. Q. Zhao, F. Li, C. Huang, *Chem. Soc. Rev.,* 2010, **39**, 3007.
52. H. Zhao, L. Zang, C. Guo, *Phys. Chem. Chem. Phys.,* 2017, **19**, 7728.

Journal Name

ARTICLE

Energy transfer and photoluminescence properties of lanthanide-containing polyoxotitanate cages coordinated by salicylate ligands

Ning Li,[a,b] Gomathy Sandhya Subramanian,[b] Peter D. Matthews,[a,c] James Xiao,[d] Vijila Chellappan,[b] Timothy E. Rosser,[a] Erwin Reisner,[a] He-Kuan Luo,[b]* and Dominic S. Wright[a]*

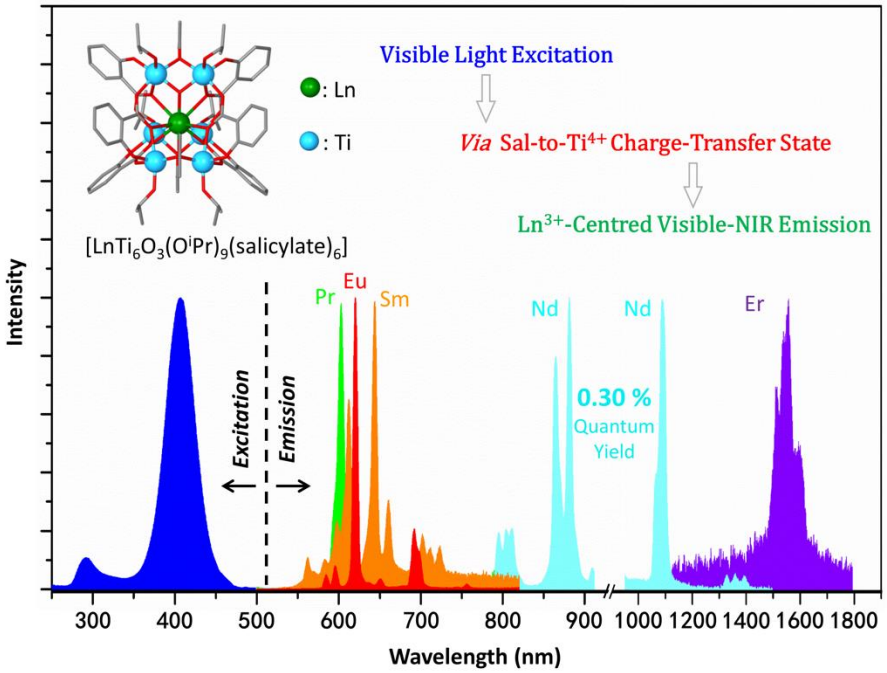

The salicylate to Ti^{4+} charge-transfer process and corresponding energy transfer mechanisms are investigated to understand the largely red-shifted Ln^{3+} photoluminescence excitation wavelengths in a series of lanthanide-containing polyoxotitanate cages.